RILEM Technical Letters (2025) 10: 68-80
https://doi.org/10.21809/rilemtechlett.2025.216

The damage rating index (DRI): A practical guideline for autonomous operator training

Cassandra Trottier[1,*], Leandro F. M. Sanchez[1]

[1]Department of Civil Engineering, University of Ottawa, Canada

Received: 13 February 2025 / Accepted: 11 September 2025 / Published online: 02 October 2025

Abstract

The damage rating index (DRI) is a microscopy tool that captures the extent of internal swelling reaction-induced deterioration (ISR). Although engineering practitioners more widely use mechanical tests, confirming the presence of ISR products through microscopy is required and standard practice. A more detailed evaluation can be achieved by combining mechanical and microscopy techniques, including the DRI, which has proven reliable in diagnosing the extent of ISR-induced deterioration. However, there is currently a lack of practical guidelines and standards in the literature explaining how to perform the DRI, raising concerns about the tool's use, particularly regarding operator variability and subjectivity. This work aims to create practical guidelines for conducting the DRI analysis methodology on concrete affected by alkali-silica reaction (ASR) originating from either reactive coarse or fine aggregates at various degrees of damage (i.e., 0.05%, 0.12%, 0.20%, and 0.30% expansion). Ranges of expected values were established to serve as autonomous training for new operators using the same reactive aggregates and mixtures.

Keywords: Alkali-silica reaction; Damage rating index; Operator training; Point-count microscopy; Damage characterization.

1 Introduction

1.1 Internal swelling reactions (ISR) in concrete: Current practices for diagnosis

Internal swelling reactions (ISR) arise from a lack of awareness and understanding of material incompatibility and the processes contributing to concrete deterioration. Industry needs, informed by research, drive education and training practices in the concrete sector; therefore, engineering practitioners are well-trained in designing concrete mixtures and structures. However, due to the age of the existing concrete infrastructure in Canada, resources (i.e., tools, literature, training, etc.) are crucial for addressing durability-related issues. Several documents (i.e., Diagnosis & Prognosis of AAR Affected Structures: State-of-the-Art Report of the RILEM Technical Committee 259-ISR; Guide to Diagnosis and Appraisal of AAR Damage to Concrete in Structures: Part 1 Diagnosis (AAR 6.1); Outil d'évaluation et de gestion des ouvrages d'art affectés de réactions alcalis-silice (RAS) ; Aide à la gestion des ouvrages atteints de réactions de gonflement interne: guide méthodologique ; and Guide to the Evaluation and Management of Concrete Structures Affected by Alkali-Aggregate Reaction [1–5] thoroughly outline theoretical concepts for using diagnostic tools; however, they do not directly guide practitioners on using and implementing these evaluation tools or interpreting the data for characterizing ISR-induced deterioration. ISR (e.g., alkali-aggregate reaction – AAR, delayed ettringite formation – DEF, freezing and thawing – F/T, etc.) are distress mechanisms that compromise the mechanical properties of concrete and its durability, deformations or deflections, an overall reduction in the service life of concrete infrastructure, and possibly leading to structural instability. While non-destructive and mechanical testing are often preferred for estimating properties of concern (i.e., compressive and tensile strengths and the modulus of elasticity), concrete petrography in this context remains among the technique used to confirm the presence of ISR. Globally, microscopy allows an operator to inspect microscopic distress features in concrete and their associated characteristics to draw conclusions based on observations. Similarly, the damage rating index (DRI) methodology and analysis can effectively capture the extent of damage at a scale that accurately represents ISR-affected concrete when conducted by a trained operator, and it can also identify the cause of deterioration when performed by an experienced professional petrographer.

*Corresponding author: Cassandra Trottier, E-mail: ctrot059@uottawa.ca

1.2 A review of the damage rating index (DRI)

The DRI is a microscopy tool used to assess concrete deterioration, where a concrete specimen or core is cut in half longitudinally and distress features counted in 1 cm by 1 cm squares marked on a flat surface using a stereomicroscope. The distress features are weighted, summed and normalized to provide a DRI number used to estimate expansion. Grattan-Bellew and Danay [6] first proposed the DRI to assess concrete cores extracted from dams exhibiting distinct deterioration levels related to alkali-silica reaction (ASR). It was established to quantify the progression of ASR relatively; however, the considered petrographic features and weighting factors were selected to emphasize signs of ASR. Since then, researchers have suggested modifications to these features and factors from a petrographic standpoint [7–9]; nonetheless, variability among operators has remained a concern regarding systematic evaluations. Villeneuve et al. (2011, 2012) subsequently tackled the issue of variability among operators, reducing the coefficient of variation to below 20% and aiming to distinguish the petrographic aspect of distress features (i.e., a crack without or with reaction products) by proposing a uniform weighting factor for these features, regardless of the presence of reaction products [10,11]. Therefore, these weighting factors most accurately represent the damage to concrete rather than merely indicating ASR, and they have been correlated with expansion [10,11]. Sanchez et al. [12,13] further examined the relationship between the DRI and mechanical responses, thereby validating the selection of the proposed weighting factors [10,11] for damage to concrete caused by ASR stemming from reactive coarse and fine aggregates down to 1 mm in size, thus confirming the applicability of the DRI methodology and analysis to reactive fine aggregates [14]. Other ISR mechanisms have been assessed using the DRI [10,15–20], attesting to its adaptability to a broader range of deterioration mechanisms.

The data collection procedure for calculating the DRI is performed on a sawn, flat, polished inner concrete surface from a core or specimen using a stereomicroscope at 15-16x magnification, where squares measuring 1 cm² are within the field of view. Distress features are counted and recorded in each square. Weighting factors related to the severity of each distress feature encountered (Table 1) are applied, and the sum of those features is calculated over 100 cm² to normalize the value, as illustrated in Equation 1.

Where CCA is the total number of closed cracks in the aggregate, $OCA\ and\ OCA_{RP}$ are the total numbers of open cracks in the aggregate without and with reaction products, respectively, DAP is the total number of disaggregated/corroded particles, $CCP\ and\ CCP_{RP}$ are the total numbers of cracks in the cement paste without and with reaction products, respectively, $Debon$ is the total number of debonded/dislodged aggregates, and *n* is the number of analyzed 1 cm² squares.

$$DRI = \frac{\sum[0.25(CCA) + 2(OCA + OCA_{RP} + DAP) + 3(CCP + CCP_{RP} + Debon)]}{n} \times 100\ cm^2 \quad (1)$$

Table 1. Pre-determined list of distress/petrographic features and associated weighting factors.

Distress/petrographic feature	Original weighting factor [6]	Updated weighting factor [10]	Type of feature
Crack in the aggregate	0.25	-	Distress
Closed crack in the aggregate (CCA)	-	0.25	Distress
Opened crack in the aggregate (OCA)	-	2	Distress
Opened crack in the aggregate with reaction products (OCA_{RP})	2	2	Distress/petrographic
Corroded/disaggregated aggregate (DAP)	-	2	Distress/petrographic
Reaction rim in aggregate	0.5	-	Petrographic
Crack in the cement paste (CCP)	2	3	Distress
Crack in the cement paste with reaction products (CCP_{RP})	4	3	Distress/petrographic
Air void lined/filled with RP	0.5	-	Petrographic
Debonded aggregate particles (Debon)	3	3	Distress

The observed data can be visualized as a plot of the DRI number as a function of expansion. In contrast, bar charts (weighted or unweighted – extended version of the DRI [12,14], discussed in section 4.1) separate distinct distress features, enabling a more diagnostic character by visualizing the proportions of features. Although complexities are associated with identifying certain crack types, especially in coarse-grained aggregates for untrained operators, the DRI remains a point-count method similar to standard procedures (e.g., ASTM C295/295M: Guide for petrographic examination of aggregates for concrete, ASTM C1356: Test Method for Quantitative Determination of Phases in Portland Cement Clinker by Microscopical Point-Count Procedure, and ASTM C457/457M: Test Method for Microscopical Determination of Parameters of the Air-Void System in Hardened Concrete) [21–23]. Nevertheless, concerns regarding operator

variability persist, which can be mitigated through adherence to a training procedure. Consequently, providing a methodology for new operators to perform such analyses autonomously is fundamental to integrating this tool into engineering practice.

2 Motivation and objective

The nuances surrounding the DRI have led to the establishment of a practical guideline for autonomous operator training on DRI methodology and analysis, further assisting engineering practitioners in evaluating damage to concrete using microscopy. This guideline presents ASR as the distress mechanism utilized for the training. The concrete mixtures were fabricated using two types of ASR-susceptible aggregates selected for their distinct deterioration patterns and variety of associated features: a reactive coarse aggregate (i.e., Springhill – Greywacke) was combined with non-reactive sand to produce ASR damage originating from the coarse aggregate, while a reactive sand (i.e., Texas – Polymictic sand) was combined with a non-reactive coarse aggregate to generate ASR damage originating from the fine aggregate. To guide the operator through various extents of damage, four levels of expansion were selected (i.e., 0.05%, 0.12%, 0.20%, and 0.30%), helping to capture the propagation of damage and its associated features. The proposed approach aims to reduce operator variability as training will be conducted on concrete under similar conditions (i.e., reactive aggregates, proportioned using standard mixtures, ASR development, and equipment for surface preparation and conducting the analysis).

3 Materials and methods

3.1 Materials and specimen fabrication

Laboratory-made cylindrical concrete specimens (i.e., 10 cm by 20 cm) are created using standard mixture proportions according to ASTM C1293-18a: Test Method for Determination of Length Change of Concrete Due to Alkali-Silica Reaction and CSA A23.2-14A: Potential expansivity of aggregates (procedure for length change due to alkali-aggregate reaction in concrete prisms at 38°C) [24,25] with a cement content of 420 kg/m^3. The characterization of aggregates and details of the mixtures are presented in Table 2 and Table 3, respectively. A reactive coarse aggregate (i.e., Springhill – Greywacke) is combined with non-reactive sand to produce ASR damage stemming from the coarse aggregate, while a reactive sand (i.e., Texas – Polymictic sand) is combined with a non-reactive coarse aggregate to generate ASR damage originating from the fine aggregate. The total alkali content of all concrete mixtures is increased to 5.25 kg/m^3 (equivalent to 1.25% Na_2O_{eq}. by cement mass) using reagent-grade NaOH to accelerate the reaction, as specified in ASTM C1293-18a and CSA A23.2-14A. The concrete specimens are then demoulded after moist curing for 24 hours (i.e., 100% RH and 20°C). Holes measuring 8 mm in diameter and 25 mm in length are drilled into both ends of the cylinders. Stainless steel screws, 19 mm in length, are used as reference points and installed in the holes with a quick-setting cement paste slurry. The concrete specimens cure for an additional 24 hours under the same conditions. Specimens are then stored after the initial length readings in environments conducive to ASR development (i.e., 100% RH and 38°C), and length change measurements are taken periodically to monitor the expansion time. It is to be noted that slight variations in the material selection and proportioning occurred to simulate such variability in different laboratories, acknowledging that materials may differ.

3.2 Sample preparation

The specimens are cut in half longitudinally with a wet masonry saw. To achieve a highly reflective surface, the suggested grinding and polishing grit sequence includes 30, 60, 140, 280 (80–100 µm), 600 (20–40 µm), 1200 (10–20 µm), and 3000 (4–8 µm). A visual guide on sample preparation for such analysis is available in [26].

3.3 The damage rating index (DRI) calculation

The DRI calculation considers all counted and weighted distress features (Table 1) by summing them, normalizing the result by dividing it by the number of analyzed squares and multiplying by 100 cm² (Equation 1). While the DRI can be applied to various ISRs, the currently proposed protocol emphasizes damage due to ASR, using the weighting factors from Villeneuve [10] in Equation 1. The distress features in the aggregates include coarse and fine aggregates [12]. Bar charts are created to separate the features and visualize their relative importance towards the overall assessment deterioration.

3.4 Referencing system and microscope set-up

A grid was utilized as a referencing system with stepping intervals of 1 cm in both the X and Y directions, which can be drawn using a fine-tip permanent marker or a 3D-printed grid. Letters and numbers are used to identify the rows and columns, respectively. Figure 1 illustrates the referencing system on a polished concrete specimen, facilitating the tabulation of observations. It is recommended to set up the spreadsheet so that the rows represent the squares under analysis and the columns reflect the categories of features while analyzing the squares from left to right. Gooseneck oblique lights illuminated the surface and highlighted the features (Figure 1).

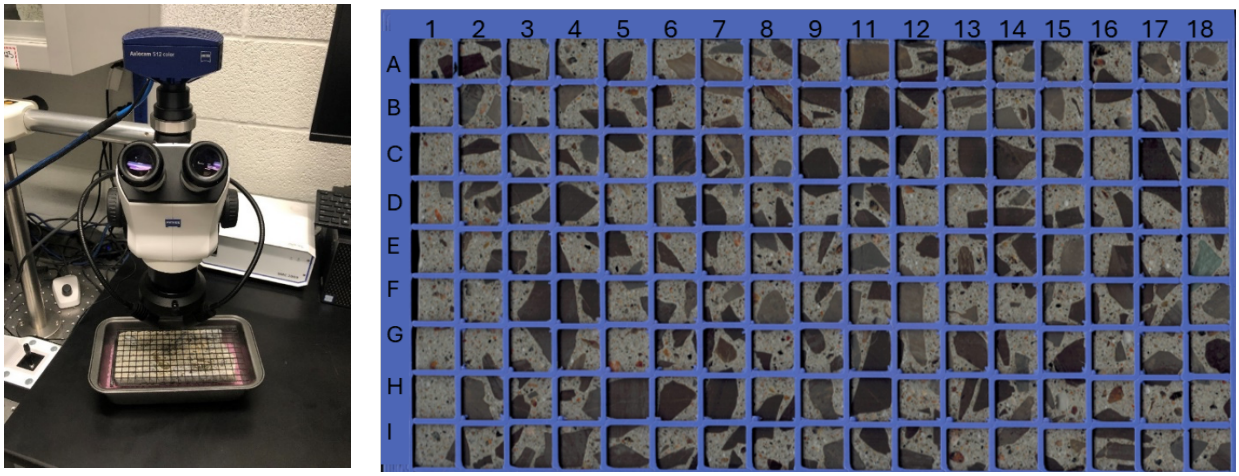

Figure 1. Stereomicroscope and specimen surface configuration.

Table 2. Aggregate characterization.

Aggregate	Location	Rock type	Relative density	Absorption (%)	Reactivity
Fine	Ottawa, Ontario (Canada)	Derived from granite	2.60-2.65	0.82-1.18	Non-reactive
Fine	Bracebridge, Ontario (Canada)	Orthoclase, Quartz, Cristoballite, Albite, Bytowmite, Cordierite, Illite, Muscovite, Larnite	2.73	0.37	Non-reactive
Fine	Ottawa, Ontario (Canada)	Manufactured crushed limestone	2.74	0.65	Non-reactive
Fine	Corpus Christie, Texas (USA)	Polymictic sand (granitic, mixed volcanics, quartzite, chert, quartz)	2.60	0.55-0.89	Reactive
Coarse	Newfoundland (Canada)	High-purity limestone	2.68	0.44	Non-reactive
Coarse	Ottawa, Ontario (Canada)	Limestone	2.78	0.42	Non-reactive
Coarse	Springhill, New Brunswick (Canada)	Greywacke	2.68-2.72	0.60-0.89	Reactive

Table 3. Mix-design per operator.

Operator	Cement	Water	Water-to-cement ratio	Non-reactive sand	Reactive coarse aggregate Springhill
				kg per 1 m³ of concrete	
1	420	189	0.45	823 (Ottawa sand)	934
2		189	0.45	860 (Bracebridge sand)	915
3		187	0.45	829 (Manufactured sand)	999
4		176	0.42	681 (Ottawa sand)	1044
5		189	0.45	836 (Ottawa sand)	938
Operator	**Cement**	**Water**	**Water-to-cement ratio**	**Reactive sand Texas**	**Non-reactive coarse aggregate**
				kg per 1 m³ of concrete	
1	420	189	0.45	760	1024 (limestone)
4		176	0.42	732	1072 (limestone)
5		189	0.45	765	1020 (limestone)
6		177	0.42	678	1093 (High-purity limestone)

3.5 Data collection

In this proposed training guide, the distress features associated with ASR damage (i.e., cracks) are listed in Table 1, and only the common features produced by the reactive Springhill and Texas aggregates will be discussed. ASR is recognizable by its cracks in the aggregate, particularly when it contains a gel-like reaction product. CCA does not exhibit an opening or gap between the edges of the crack (Figures 2a to d). OCA and OCA_{RP} present an opening between the crack edges and can be either empty or filled with reaction products, respectively (Figures 2e and f). A partially filled OCA is regarded as an OCA_{RP}, while a combination of CCA and OCA may be observed on a single crack segment (Figures 2g and h, respectively). CCP and CCP_{RP} refer to those within the bulk cement paste (Figure 2i). An OCA or OCA_{RP} that extends from the aggregate to the cement paste is counted as two distinct crack types (Figures 2j to l).

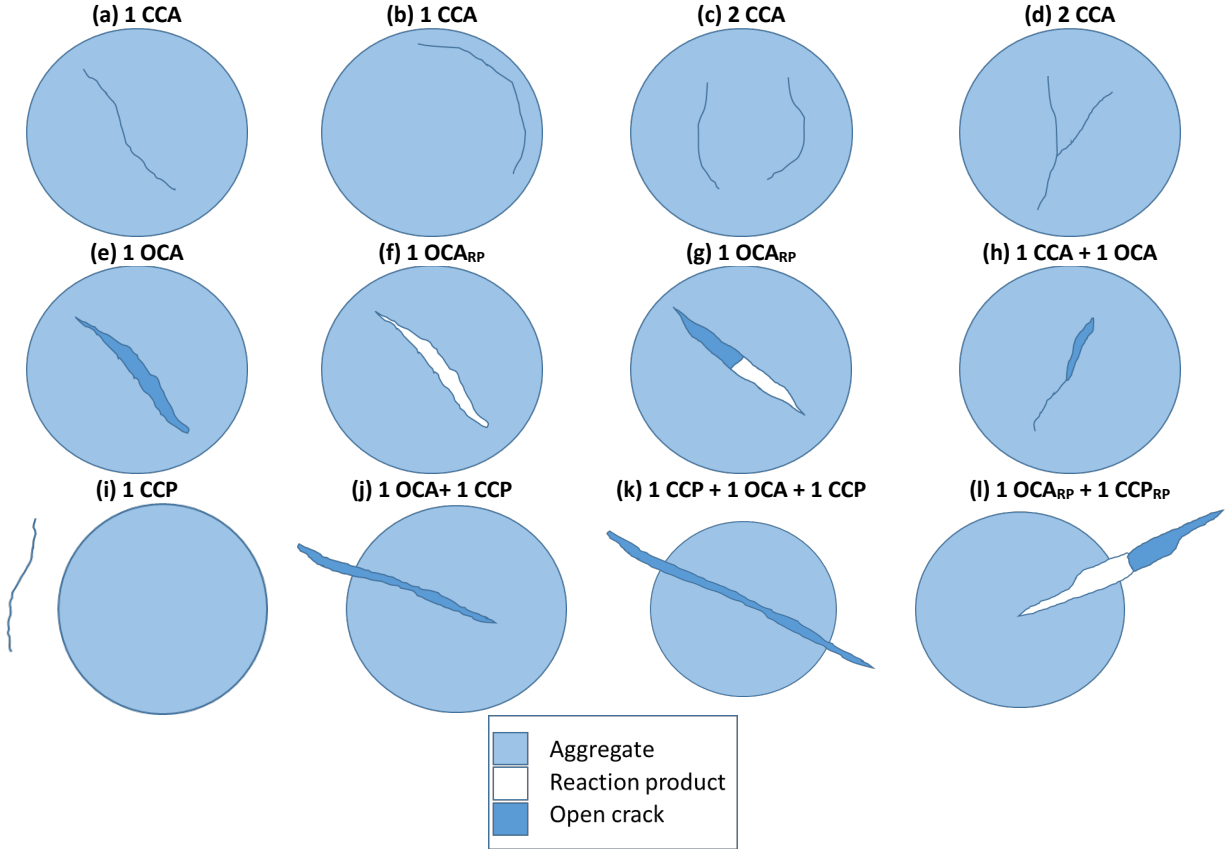

Figure 2. Crack type and counts schematics.

Multiple connected cracks can be observed; therefore, the point-counting technique applied to cracks in networks is illustrated in Figure 3. In practice, cracks are counted starting from one segment tip (starting point) and following the crack until all ends have been considered (endpoints indicated by numbers).

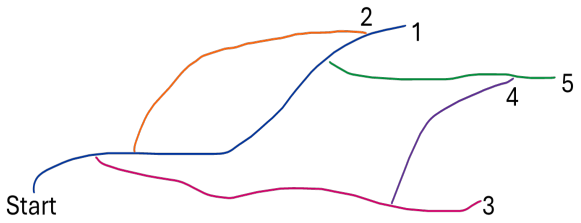

Figure 3. Counts in a crack network.

For instance, in Figure 4a, the CCP links two OCA_{RP}. Figure 4b presents a longer CCP present in the bulk cement paste, in the aggregate-paste interface, and a crack connecting several reactive sand particles through the cement paste. Figure 4c illustrates a CCA and natural veins in the aggregate. Furthermore, in the images, natural veins and cracks can easily be confused; however, their appearance under the microscope with proper lighting conditions reveals their distinctive characteristics, where depth is noticeable in an OCA. The reactive sand used in this work is shown in Figure 4d, where the OCA and CCP can be observed. More examples of micrographs can be found in the literature [10,12,27].

4 Proposed approach

4.1 A new perspective on the analysis of DRI results

The DRI is typically represented as a number or through bar charts to differentiate the various distress features. Sanchez et al. [12,14] proposed an extended version of the DRI, which includes unweighted counts per 100 cm² and proportions to aid in damage propagation analyses. Figures 5a and 5b illustrate the lower and upper limits of the DRI numbers as a function of expansion and as bar charts, respectively. The DRI numbers increase with expansion; however, overlap is observed between adjacent expansion levels' lower and upper limits. Overall, the differences in DRI numbers between the lower and upper limits grow with expansion. DRI numbers of 136 and 201 were determined at 0.05% expansion and differences of 419 and 614 at 0.30% expansion for the Springhill reactive coarse aggregate and Texas reactive sand, respectively. These differences are significant when assessing the extent of damage due to ASR; therefore, it is necessary to break down the distress features into bar charts to better understand their propagation and distribution. The operators' combined unweighted counts and proportions as lower and upper limits (i.e., the minimum and maximum values obtained) are illustrated in Figure 5c and 5d. The CCA typically accounts for over 45% of the distress features, followed by the OCA+OCA_{RP}, which ranges from 23% to 46% and 6% to 37% for Springhill and Texas, respectively. The CCP+CCP_{RP} is less prevalent because the distress mechanisms are more common in the aggregates, at 3% to 14%. Similarly, the OCA+OCA_{RP} and CCP+CCP_{RP} increase with expansion, yet the results overlap.

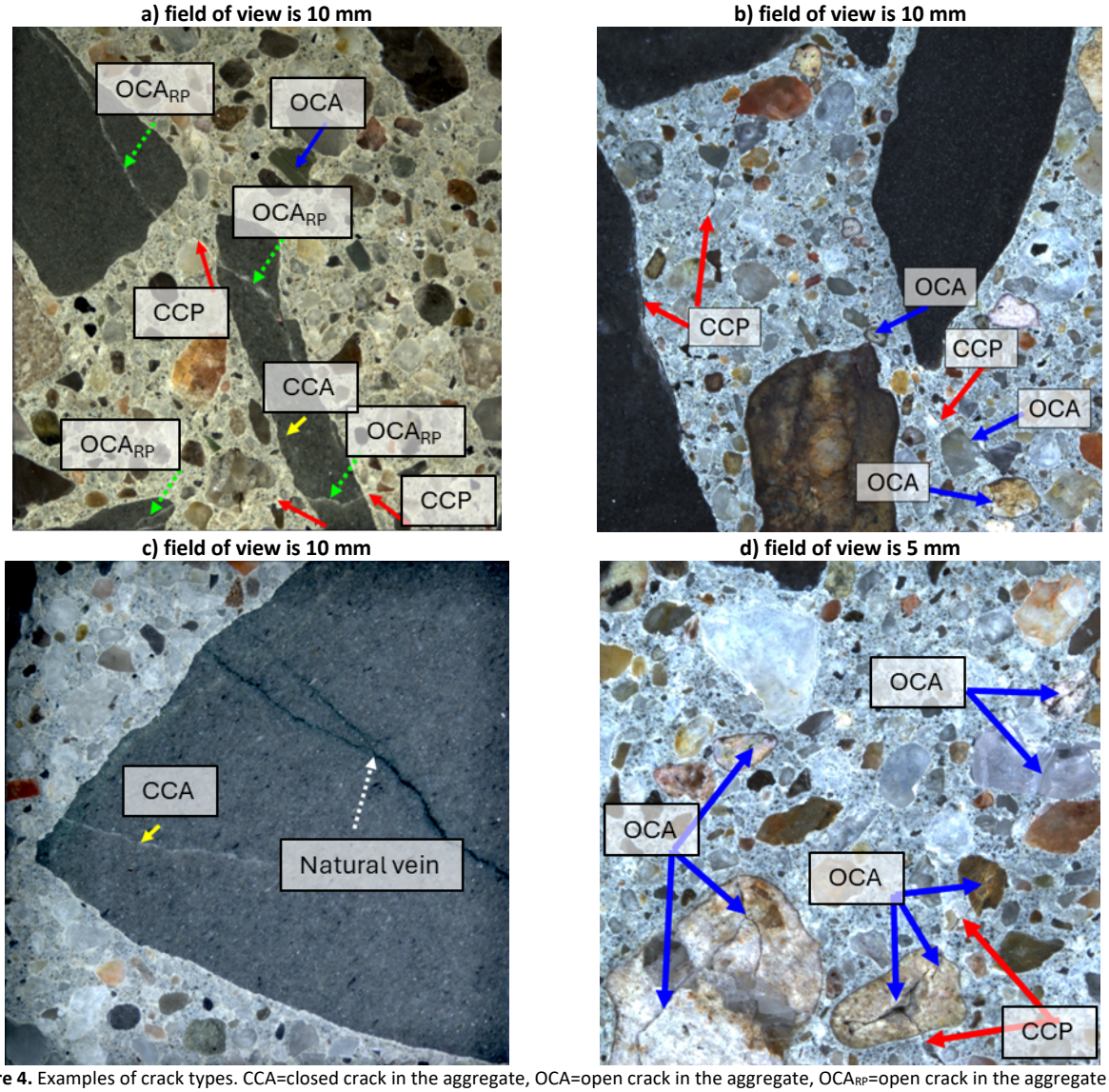

Figure 4. Examples of crack types. CCA=closed crack in the aggregate, OCA=open crack in the aggregate, OCA_{RP}=open crack in the aggregate with reaction product, CCP=crack in the cement paste, and CCP_{RP}=crack in the cement paste with reaction product.

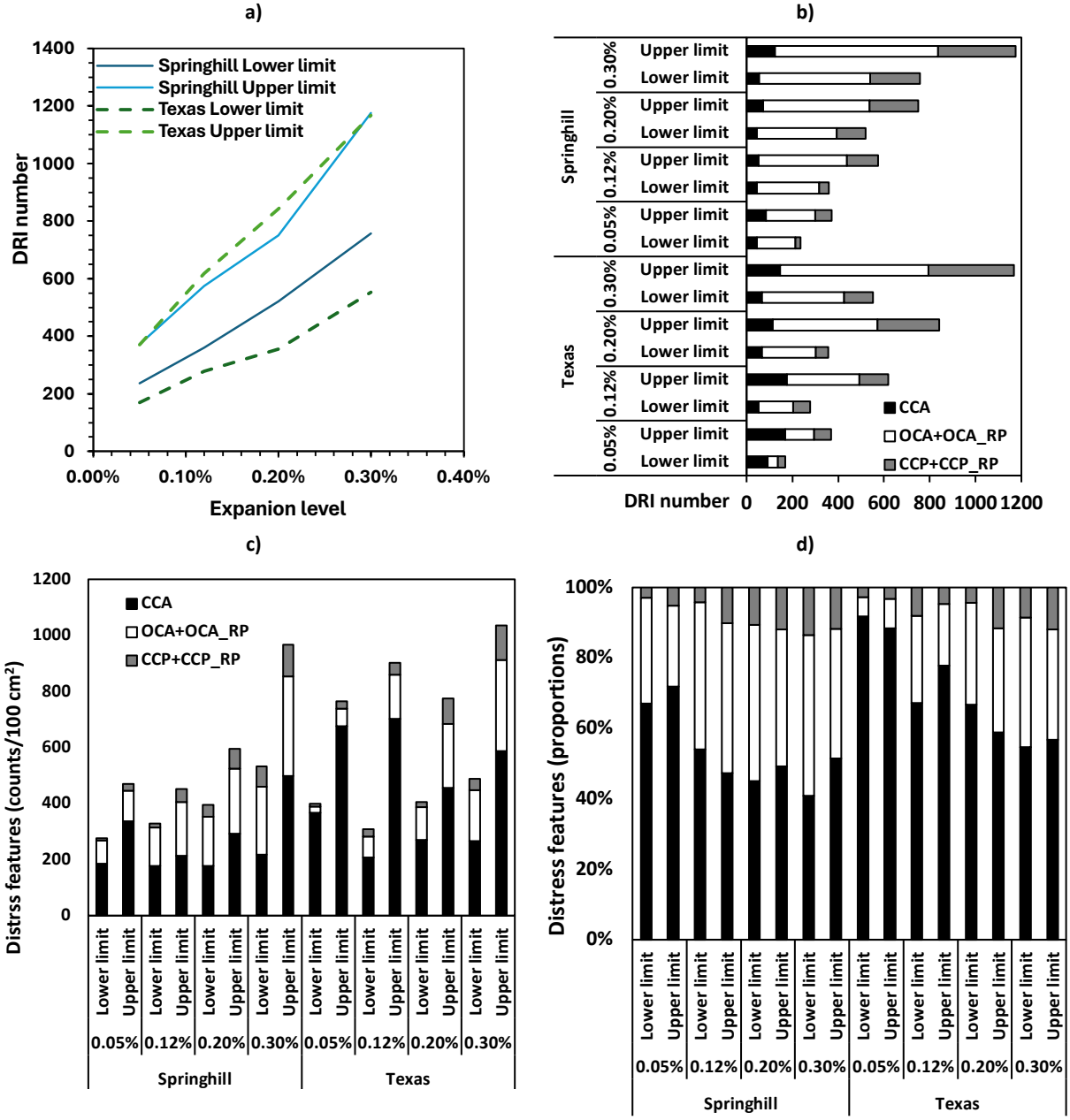

Figure 5. The DRI as a function of expansion is presented as a) the DRI number obtained for all operators, b) weighted bar charts, c) an extended version of the DRI as c) counts/100 cm^2 and d) proportions. CCA=closed crack in the aggregate, OCA=open crack in the aggregate, OCA_{RP}=open crack in the aggregate with reaction product, CCP=crack in the cement paste, and CCP_{RP}=crack in the cement paste with reaction product.

The observed count data was broken down into histograms for each distress feature (i.e., CCA, OCA+OCA_{RP}, and CCP+CCP_{RP}) and reactive aggregate type (Figure 6), where the frequencies of counts (y-axis) are displayed as a function of count categories (x-axis), with the categories representing the number of instances a certain distress feature was counted in each square. The histograms showcase the results from all operators combined, illustrating their sensitivity to various expansion levels. The maximum count category increases with expansion, as evidenced by the longer and thicker tail. The shapes of the histograms differ for the CCA when comparing the aggregate type, with means ranging from 1.95 to 3.56 and 4.02 to 4.95 for the Springhill and Texas reactive aggregates, respectively. The means for OCA+OCA_{RP} (referenced as OCA in Figure 6) also increase with expansion, ranging from 0.98 to 2.9 and 0.54 to 2.31 for the Springhill and Texas reactive aggregates, respectively. The OCA+OCA_{RP} for the Springhill aggregate exhibits a decreasing frequency from zero counts at 0.05% expansion, an increase from 0 to 1 count at 0.12% expansion, a consistent slope from 0 to 2 counts at 0.20% expansion, and a peak at 3 counts for the 0.30% expansion. Conversely, OCA+OCA_{RP} for the Texas sand at 0.05%, 0.12%, and 0.20% expansion shows a decrease in frequency from zero count and peaks at 1 count for the 0.30% expansion. The CCP+CCP_{RP} (referenced as CCP in Figure 6) decreases frequencies from zero counts for the Springhill and Texas aggregates, with means ranging from 0.14 to 1.01 for the Springhill aggregate and 0.16 to 0.86 for the Texas sand.

Furthermore, the magnitude of frequencies varies by reactive aggregate type, thereby highlighting the histogram's capacity to capture these differences.

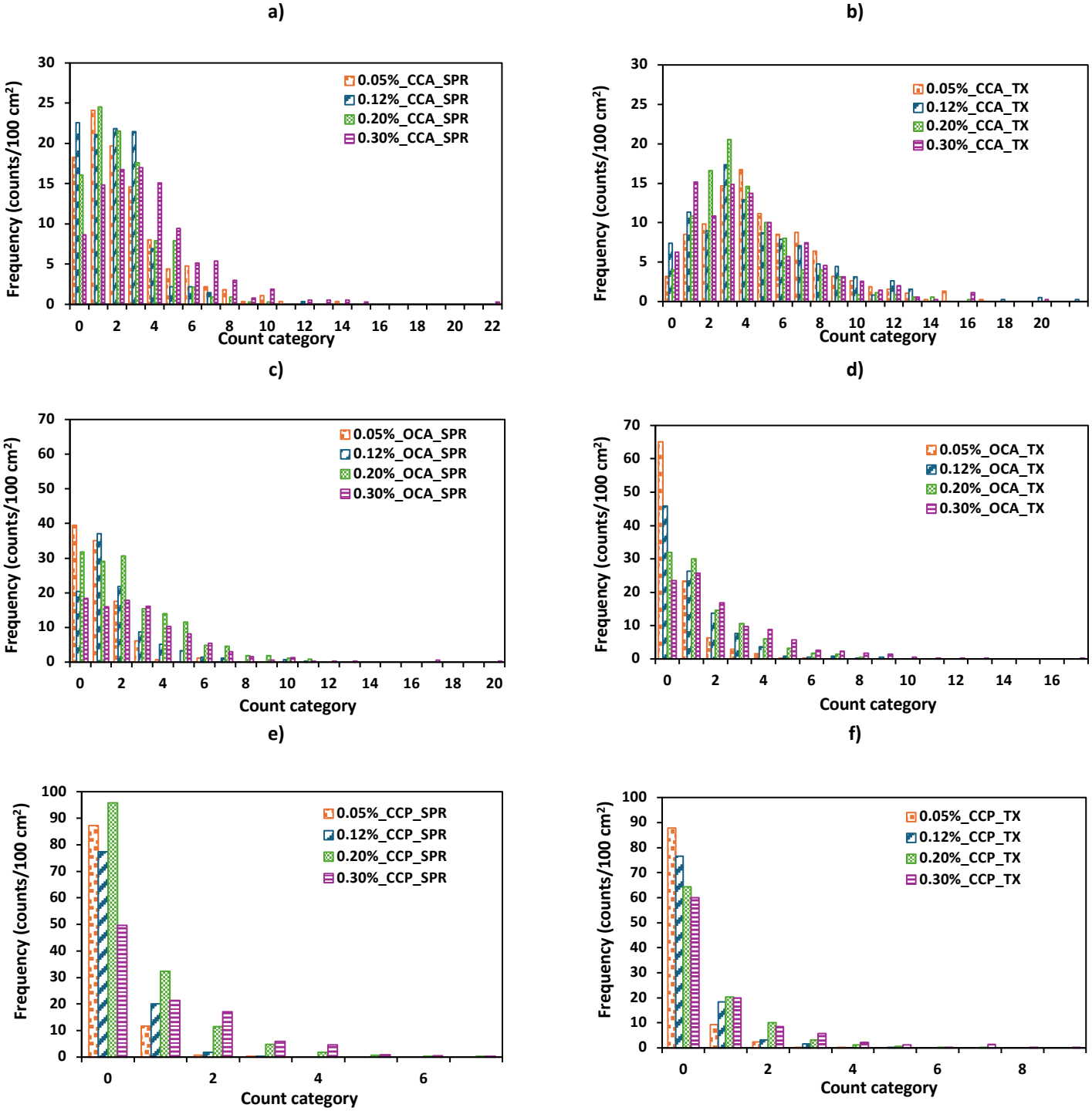

Figure 6. Histograms of distress feature counts per reactive aggregate type. CCA=closed crack in the aggregate, OCA=open crack in the aggregate, CCP=crack in the cement paste, SPR=Springhill, and TX=Texas

4.2 Autonomous operator training

Operator-dependent testing can lead to patterns requiring acceptable value ranges for each distress feature category. Moreover, during training, histograms can help eliminate encountered biases and ensure that operator counts align with the distribution of expected counts rather than over or under-compensating to achieve a desired result. Consequently, the data collected from operators was used to create cumulative curves with lower and upper-value limits to establish the acceptable ranges a new operator should achieve when assessing ASR damage to concrete derived from Springhill and Texas reactive aggregates (Tables 4 and 5, respectively). These tables outline the lower and upper limits for the total counts, as the operator is expected to remain within these total counts and within the cumulative frequency ranges.

Table 4. Cumulative count frequencies for Springhill coarse aggregate.

	Expansion level	0.05%						0.12%					
	Distress feature	CCA		OCA+OCA$_{RP}$		CCP+CCP$_{RP}$		CCA		OCA+OCA$_{RP}$		CCP+CCP$_{RP}$	
	Limits	Lower	Upper	Lower	Upper	Lower	Upper	Lower	Upper	Lower	Upper	Lower	Upper
	Counts/100 cm^2	185	337	83	108	8	24	177	213	137	192	14	46
Count category	0	5.7	26.0	38.1	40.2	78.1	92.9	7.6	31.8	3.8	30.6	57.1	90.0
	1	20.0	56.2	70.4	81.0	98.8	99.0	29.5	52.4	51.8	66.7	97.1	97.6
	2	42.9	74.0	88.2	98.1	99.0	100.0	60.0	68.8	71.2	92.4	98.8	100.0
	3	61.0	86.4	97.0	100.0	100.0		84.1	91.4	80.6	100.0	99.4	
	4	73.3	91.7	98.2				91.2	98.1	88.8		100.0	
	5	82.9	92.9	98.2				93.5	100.0	94.1			
	6	89.5	96.5	100.0				97.1		96.5			
	7	93.3	97.6					99.4		98.2			
	8	97.1	98.2					99.4		98.2			
	9	98.1	98.2					99.4		98.2			
	10	99.1	99.4					99.4		99.4			
	11	100.0	99.4					99.4		100.0			
	12		99.4					100.0					
	13		99.4										
	14		100.0										

	Expansion level	0.20%						0.30%					
	Limits	Lower	Upper	Lower	Upper	Lower	Upper	Lower	Upper	Lower	Upper	Lower	Upper
	Counts/100 cm^2	178	293	175	232	42	71	217	498	243	356	72	113
Count category	0	2.9	22.7	19.1	34.5	50.5	68.9	2.7	21.0	10.2	30.3	44.9	53.3
	1	26.7	47.2	44.3	51.3	81.5	92.5	11.6	46.2	23.8	50.4	66.4	80.0
	2	46.7	74.0	58.5	78.1	89.9	98.1	24.5	62.2	40.1	67.2	84.0	95.2
	3	71.4	85.7	71.7	90.5	95.0	100.0	39.5	75.6	57.8	76.5	89.9	99.0
	4	79.1	95.8	83.0	93.3	97.5		54.4	88.2	71.4	85.7	97.5	100.0
	5	91.4	99.2	91.5	98.1	98.3		63.3	94.1	81.0	95.2	98.3	
	6	94.3	99.2	95.3	100.0	99.7		71.4	97.1	88.4	97.1	99.2	
	7	96.2	100.0	98.1		100.0		81.0	100.0	91.8	100.0	100.0	
	8	99.1		99.1				87.8		95.0			
	9	99.1		99.1				89.8		95.2			
	10	100.0		99.1				94.6		97.3			
	11			100.0				94.6		98.0			
	12							95.9		98.3			
	13							97.3	13-18	98.6-98.6			
	14							98.6	19	99.2			
							15-21	99.3-99.3	20	100.0			
							22	100.0					

Table 5. Cumulative count frequencies for Texas fine aggregate.

	Expansion level	0.05%						0.12%					
	Distress feature	CCA		OCA+OCA$_{RP}$		CCP+CCP$_{RP}$		CCA		OCA+OCA$_{RP}$		CCP+CCP$_{RP}$	
	Limits	Lower	Upper	Lower	Upper	Lower	Upper	Lower	Upper	Lower	Upper	Lower	Upper
	Counts/100 cm^2	367	676	22	63	11	25	207	702	76	158	25	42
Count category	0	2.8	3.8	47.6	83.6	79.0	91.5	1.9	18.3	30.8	58.8	60.6	82.9
	1	9.4	15.2	77.4	97.6	96.2	97.6	1.9	50.0	56.7	81.2	94.1	97.1
	2	16.0	26.7	86.8	98.1	98.8	100.0	8.5	60.6	76.9	90.6	97.1	100.0
	3	23.6	47.6	100.0	100.0	99.4		16.0	84.6	89.4	95.3	99.4	
	4	34.9	68.6			100.0		31.1	91.3	94.3	98.8	99.4	
	5	43.4	82.9					37.7	97.1	96.2	99.4	100.0	
	6	49.1	93.3					50.0	97.1	97.1	100.0		
	7	62.3	96.2					63.2	98.1	98.1			
	8	68.9	99.0					71.7	98.1	99.0			
	9	74.5	100.0					77.4	99.0	100.0			
	10	79.2						85.8	99.0				
	11	84.0						86.8	100.0				
	12	89.6						92.5					
	13	93.4					13-21	96.2-96.2					
	14	94.3					22	100.0					
	15-16	99.1-99.1											
	17	100.0											

	Expansion level	0.20%						0.30%					
	Limits	Lower	Upper	Lower	Upper	Lower	Upper	Lower	Upper	Lower	Upper	Lower	Upper
	Counts/100 cm^2	271	455	117	229	18	90	267	588	180	324	42	124
Count category	0	3.8	4.1	17.1	39.5	47.3	82.9	3.9	8.6	7.6	34.2	50.9	76.3
	1	9.2	26.7	41.0	72.8	74.0	99.0	9.2	41.0	28.6	58.0	72.2	88.2
	2	23.7	48.6	61.0	84.0	91.7	100.0	17.1	57.1	44.8	75.7	80.5	97.4
	3	36.8	75.2	75.2	93.5	94.7		31.6	69.5	59.0	83.4	88.8	100.0
	4	55.3	85.7	88.6	97.6	96.1		46.1	83.8	74.3	89.9	93.5	
	5	61.8	94.3	94.3	98.2	97.4		52.6	86.7	82.9	95.3	95.9	
	6	69.7	96.2	95.2	99.4	98.7		57.9	92.4	87.6	97.0	95.9	
	7	78.9	99.0	98.7	100.0	100.0		71.1	96.2	90.8	97.6	98.8	
	8	85.5	99.0	100.0				77.6	99.0	93.4	98.1	99.4	
	9	89.5	100.0					82.9	99.0	96.1	99.0	100.0	
	10	90.8						86.8	100.0	97.4	100.0		
	11	93.4						90.8		97.4			
	12	94.7						93.4	12-16	98.7-98.7			
	13	96.1						96.1	17	100.0			
	14	98.7					14-19	97.4-97.4					
	15	98.7					20	100.0					
	16	100.0											

4.3 Representative sample size

The number of analyzed 1 cm² squares was also considered to ensure that the DRI values were derived from a representative sample. Convergence (approaching a slope of ± 20 DRI units) was noted through the law of large numbers (Equation 2) from cumulative DRI values as a function of the number of analyzed squares (Figure 7).

$$DRI = \frac{\sum_{i=1}^{n} X_i}{n} = \frac{X_1 + X_2 + X_3 + \cdots + X_n}{n} \quad (2)$$

Where X_i represents the DRI number until square i and n is the total number of analyzed squares.

This cumulative concept confirmed what constitutes a representative sample based on 1 cm² squares rather than multiple concrete specimens. This ensures that the operator's DRI number converges toward a mean value, provided the damage is homogeneous across the analyzed surface. Convergence was achieved at a smaller *n* for lower expansion levels. Larger sample sizes are necessary for higher expansion levels, where the average surface area needed to reach convergence for the Springhill coarse aggregate was 21, 35,

46, and 65 cm², at expansion levels of 0.05%, 0.12%, 0.20%, and 0.30%, respectively. In contrast, 21, 52, 51, and 64 cm² were required for the Texas fine aggregate at expansion levels of 0.05%, 0.12%, 0.20%, and 0.30%, respectively. This indicates that the sample size partially depends on the observed level of damage and the source of ASR damage. Therefore, a sample size of 100 cm² for laboratory-made specimens is sufficient to capture all extent of ASR-induced deterioration [14]. However, concrete extracted from field structures requires further studies to understand better the varying patterns caused by external and internal factors. Consequently, a minimum of 200 cm² remains the suggested sample size for extracted cores from the field concrete, provided convergence is met.

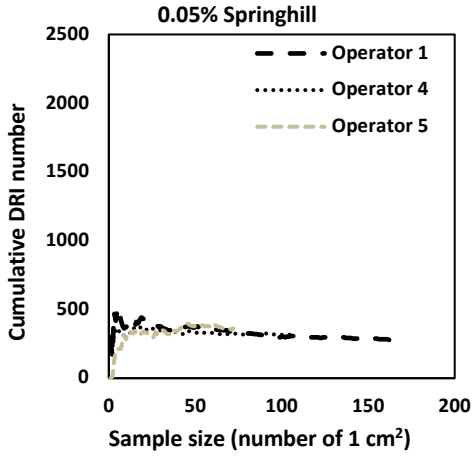

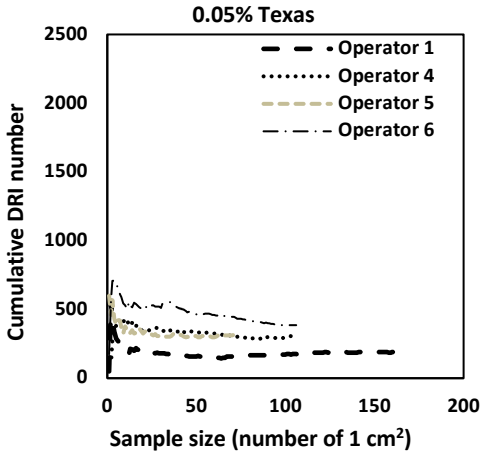

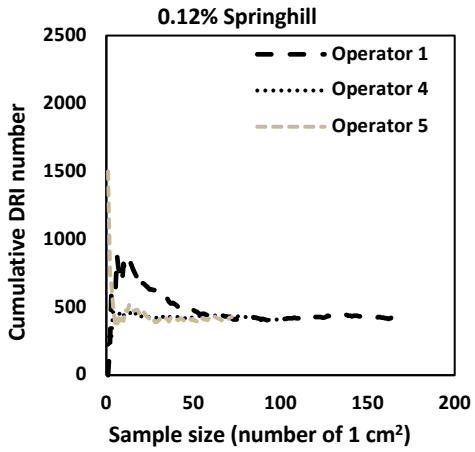

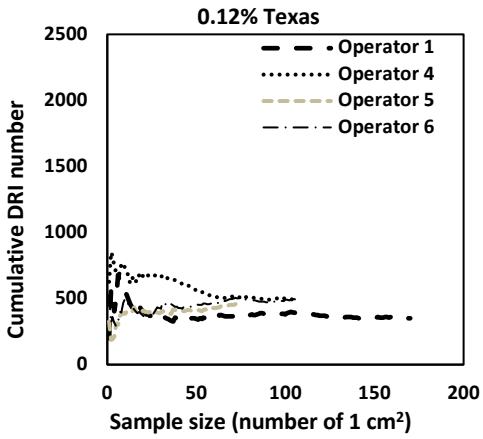

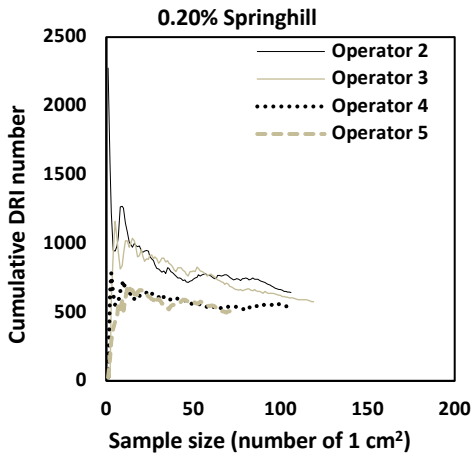

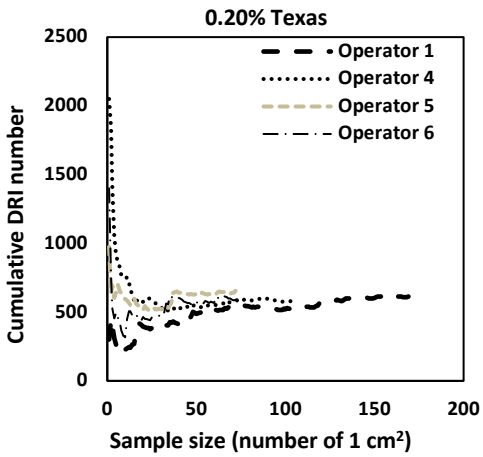

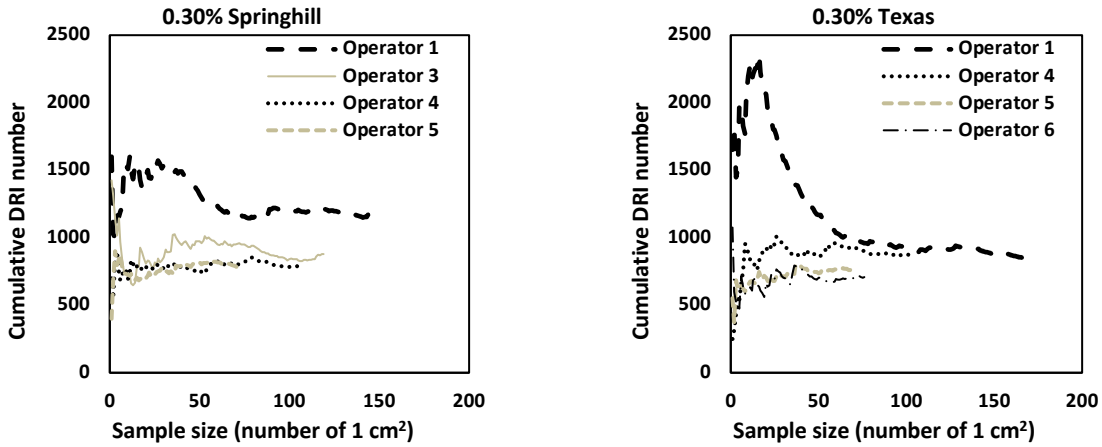

Figure 7. Convergence plots.

5 Concluding remarks and future perspectives

When viewed as a tool rather than purely a numerical output, the DRI can provide valuable information into the cause(s) and extent of damage in affected concrete. This guide aims to facilitate the adoption of the DRI technique with reduced variability and subjectivity introduced by the operator. The proposed method builds upon an extended version of the DRI [12,14], utilizing unweighted counts, histograms illustrating the frequency of plotted count categories, and calculated means. These histograms have demonstrated to be influenced by the various damage levels. They can establish acceptable value ranges for operators when autonomously training and assessing ASR damage to concrete across various degrees of damage. Further research is required to incorporate additional aggregate types into the training portfolio and other forms of ISR for a more comprehensive approach to characterizing the extent of ISR-induced deterioration with respect to its cause using the DRI. This tool offers an opportunity to include microscopy for informed engineering decision-making.

Authorship statement (CRediT)

Cassandra Trottier: Conceptualization, Methodology, Validation, Formal analysis, Investigation, Writing – Original Draft, Visualization. **Leandro F. M. Sanchez:** Resources, Writing – Review & Editing, Supervision.

Acknowledgements

The authors thank the operators for providing their data: Mayra T. de Grazia, Olusola David Olajide, Andisheh Zahedi, and Diego Jesus De Souza. They also acknowledge the financial support of the prestigious Vanier scholarship funded by NSERC (Natural Sciences and Engineering Research Council of Canada), from which Cassandra Trottier benefitted.

References

[1] V.E. Saouma, ed., Diagnosis & Prognosis of AAR Affected Structures: State-of-the-Art Report of the RILEM Technical Committee 259-ISR, Springer International Publishing, Cham, 2021. https://doi.org/10.1007/978-3-030-44014-5

[2] B. Godart, M. De Rooij, J.G.M. Wood, eds., Guide to Diagnosis and Appraisal of AAR Damage to Concrete in Structures: Part 1 Diagnosis (AAR 6.1), Springer Netherlands, Dordrecht, 2013. https://doi.org/10.1007/978-94-007-6567-2

[3] M.-A. Bérubé, N. Smaoui, B. Bissonnette, B. Fournier, Outil d'évaluation et de gestion des ouvrages d'art affectés de réactions alcalis-silice (RAS), Ministère des transports du Québec, Québec, 2005.

[4] Laboratoire central des ponts et chaussées, ed., Aide à la gestion des ouvrages atteints de réactions de gonflement interne: guide méthodologique, Laboratoire central des ponts et chaussées, Paris, 2003.

[5] CSA A864-00 (R2005), Guide to the Evaluation and Management of Concrete Structures Affected by Alkali-Aggregate Reaction, (2005). https://www.csagroup.org/store/product/A864-00/.

[6] P.E. Grattan-Bellew, A. Danay, Comparison of laboratory and field evaluation of alkali- silica reaction in large dams, in: Collection / Collection : NRC Publications Archive / Archives des publications du CNRC, 1992: pp. 1-25.

[7] G.G. Clemena, S. Lane, T. Freeman, M. Lozev, Evaluation of nondestructive evaluation methods for application in early detection of deterioration in concrete pavements, VTRC 00-R13, Virginia Transportation Research Council, Charlottesville, USA, 2000. https://rosap.ntl.bts.gov/view/dot/14227.

[8] L. Powers, F.H. Shrimer, Quantification of ASR in concrete: an introduction to the Damage-Rating method, in: 29th International Conference on Cement Microscopy, Québec, Canada, 2007.

[9] N. Smaoui, M.-A. Bérubé, B. Fournier, B. Bissonnette, B. Durand, Evaluation of expansion attained by ASR-affected concrete, in: 12th International Conference on Alkali-Aggregate Reaction, Beijing, China, 2004: pp. 1005-1015.

[10] V. Villeneuve, Détermination de l'endommagement du béton par méthode pétrographique quantitative, Master's Thesis., Université Laval, 2011.

[11] V. Villeneuve, B. Fournier, J. Duchesne, Determination of the damage in concrete affected by ASR - the damage rating index (DRI), in: 14th International Conference on Alkali-Aggregate Reaction, Texas, USA, 2012.

[12] L.F.M. Sanchez, B. Fournier, M. Jolin, J. Duchesne, Reliable quantification of AAR damage through assessment of the Damage Rating Index (DRI), Cement and Concrete Research 67 (2015) 74-92. https://doi.org/10.1016/j.cemconres.2014.08.002

[13] L.F.M. Sanchez, B. Fournier, M. Jolin, D. Mitchell, J. Bastien, Overall assessment of Alkali-Aggregate Reaction (AAR) in concretes presenting different strengths and incorporating a wide range of reactive aggregate types and natures, Cement and Concrete Research 93 (2017) 17-31. https://doi.org/10.1016/j.cemconres.2016.12.001

[14] L.F.M. Sanchez, B. Fournier, M. Jolin, M.A.B. Bedoya, J. Bastien, J. Duchesne, Use of Damage Rating Index to Quantify Alkali-Silica Reaction Damage in Concrete: Fine versus Coarse Aggregate, ACI Materials Journal 113 (2016). https://doi.org/10.14359/51688983

[15] M.-A. Bérubé, B. Fournier, T. Côté, Using the damage rating index for assessing the expansion of concrete affected by freeze-thaw, sulphate attack, or ASR, in: 14th International Conference on Alkali-Aggregate Reaction, Austin, Texas, USA, 2012.

[16] L.F.M. Sanchez, T. Drimalas, B. Fournier, D. Mitchell, J. Bastien, Comprehensive damage assessment in concrete affected by different internal swelling reaction (ISR) mechanisms, Cement and Concrete Research 107 (2018) 284-303. https://doi.org/10.1016/j.cemconres.2018.02.017

[17] L.F.M. Sanchez, T. Drimalas, B. Fournier, Assessing condition of concrete affected by internal swelling reactions (ISR) through the Damage Rating Index (DRI), Cement 1-2 (2020) 100001. https://doi.org/10.1016/j.cement.2020.100001

[18] P.E. Grattan-Bellew, Petrographic methods for distinguishing between alkali- silica, alkali-carbonate reactions and other mechanisms of concrete deterioration, in: Proceedings of the 14th International Conference on Alkali-Aggregate Reaction in Concrete, Austin, Texas, USA, 2012.

[19] R.-P. Martin, L. Sanchez, B. Fournier, F. Toutlemonde, Evaluation of different techniques for the diagnosis & prognosis of Internal Swelling Reaction (ISR) mechanisms in concrete, Construction and Building Materials 156 (2017) 956-964. https://doi.org/10.1016/j.conbuildmat.2017.09.047

[20] I. Zahedi, A. Komar, L.F.M. Sanchez, A.J. Boyd, Global assessment of concrete specimens subjected to freeze-thaw damage, Cement and Concrete Composites 133 (2022) 104716. https://doi.org/10.1016/j.cemconcomp.2022.104716

[21] ASTM International, ASTM C295/295M:19 Guide for Petrographic Examination of Aggregates for Concrete, ASTM International, West Conshohocken, PA, USA, 2019. https://doi.org/10.1520/C0295_C0295M-19

[22] ASTM International, ASTM C457/457M:16 Test Method for Microscopical Determination of Parameters of the Air-Void System in Hardened Concrete, (2016). https://doi.org/10.1520/C0457_C0457M-16

[23] ASTM International, ASTM C1356-07: Test Method for Quantitative Determination of Phases in Portland Cement Clinker by Microscopical Point-Count Procedure, (2020). https://doi.org/10.1520/C1356-07R20

[24] ASTM C1293-18a, Test Method for Determination of Length Change of Concrete Due to Alkali-Silica Reaction, (2018). https://doi.org/10.1520/C1293-18A

[25] CSA A23.2-14A Potential expansivity of aggregates (procedure for length change due to alkali-aggregate reaction in concrete prisms at 38 °C), (2019).

[26] L.F.M. Sanchez, Internal Swelling Reactions in Concrete: Mechanisms and Condition Assessment, 1st ed., CRC Press, Boca Raton, 2024. https://doi.org/10.1201/9781003188155

[27] M. Champagne, Applying the damage rating index for the spatial damage assessment in concrete specimens affected by alkali-silica reaction (ASR), Master's Thesis., Université Laval, 2020.